Evaluating the Resilience of Superhydrophobic Materials using the Slip Length Concept

H Xu[1], C R Crick*[2] and R J Poole[1]

[1]School of Engineering, University of Liverpool, Liverpool, L69 3GH, United Kingdom

[2]Department of Chemistry, University of Liverpool, Liverpool, L69 7ZD, United Kingdom

* *Corresponding Author* - c.crick@liverpool.ac.uk

Abstract

The drive to introduce superhydrophobic materials into real-world applications requires the development of robust and effective surfaces. Efforts to formulate a collective understanding of the design approaches required to engineer resilience are hindered significantly by inconsistencies in the evaluation methods used throughout the literature. Herein, we report a technique that accurately quantifies both the superhydrophobicity, and superhydrophobic resilience under fluid shear stress, using slip-length measurements. Two types of superhydrophobic surface are used (micro-rough PTFE, and nano/micro-rough nanoparticle coatings), in order to demonstrate the different mechanisms of superhydrophobic degradation, in addition to the versatility of the slip-length technique to study the phenomena. The shear stress testing is symptomatic of real-world conditions (applied fluid stress), an environment where superhydrophobic materials are relatively vulnerable due to their comparative fragility. The technique is both a comprehensive, sensitive and quantitatively reproducible, assessment method of superhydrophobic interfaces, which if widely adopted, would accelerate progress in this area.

1. Introduction

The widespread implementation of highly water repellent (superhydrophobic) materials is contingent on their ability to function continually under real-world conditions.[1] This has proved a stumbling block for many materials reported in the scientific literature,[2] despite demonstrating highly beneficial functional properties (self-cleaning, anti-biofouling, and water purification – in addition to others).[3–9] Current commercial success of superhydrophobic materials focuses on short-to-medium term surface treatments, which require recurrent reapplication to maintain their functional properties.[10] As a result, improving robustness and extending the longevity of superhydrophobic materials through targeted design is an intense area of research.[11]

A range of approaches has been reported in the fabrication of superhydrophobic materials, however the surface properties required to produce extreme water repulsion are generally consistent. Superhydrophobic materials must possess a highly rough surface morphology (micro/nanoscale), in addition to an inherently hydrophobic surface chemistry (e.g. alkyl, or fluorocarbon functionality).[12-16] The static water contact angle (WCA) provides the most often used direct method in quantifying surface hydrophobicity. This is the angle made by the plane of the surface and the tangent made by a water droplet at the air-water-surface interface, whereby hydrophobic surfaces have a WCA above 90°, and superhydrophobic surfaces are those possessing a WCA over approximately 150°.[17] Well established surface models (Wenzel – fully wetted, and Cassie-Baxter – partially wetted) can be used to both predict and rationalise surface wetting behaviour, through consideration of surface energy, roughness, and the prevalence of a trapped air layer.[18,19] However, improvements in superhydrophobic performance can be achieved through further enhancing surface roughness, and/or by increasing the hydrophobicity of the surface chemistry. This has the effect of intensifying the water repulsion, while facilitating the trapping of air underneath any water contacting the surface.[20] This air allows for very low adhesion, water moving easily across the surface of superhydrophobic materials, and potential "drag reduction" in fluid dynamics applications.[21]

The two major factors limiting the real-world implementation of superhydrophobic materials are; (i) degradation/removal of surface roughness – caused by the fragility of small (micro/nanoscale) surface features, and (ii) the loss of trapped air from the water-surface interface upon extended use or exposure to high fluid shear stress or even to turbulent-flow forces.[22,23] Both have the effect of severely reducing surface hydrophobicity, and can be

quantified through a reduction in the static WCA, and change in wetting/de-wetting behaviour (i.e. tilt angle, or WCA hysteresis). The tilt angle is a measure of how far from horizontal a surface may be tilted before a water droplet on the surface begins to move. WCA hysteresis is a related measurement, but is defined at the difference between the advancing and receding WCAs.[24] Although there has been a tremendous amount of research dedicated to the examination of superhydrophobic surface degradation,[10,25–35] there is an absence of an overarching testing consistency, or use of statistically indeterminate observations (e.g. removal of material with adhesive tape – scotch tape test).[36] As a result, the comparison of materials reported in the literature, and their resultant real-world applicability, is generally a challenging prospect.

The work presented introduces a fully-quantifiable method for assessing the robustness and longevity of superhydrophobic materials to applied fluid shear stress. Providing a real-time measure of the dynamic interaction between water and these surfaces, which is not afforded by monitoring static WCAs, and wetting/de-wetting methods, or inspection of surface damage *via* microscopy. The technique employs continual controlled flow(/fluid stress) testing utilising a cone-and-plate geometry on a conventional controlled-stress rheometer (Figure 1), allowing constant monitoring of the so-called "slip-length".[1] The slip-length is a measure of the potential drag-reducing properties of superhydrophobic materials, caused by the layer of trapped air at the water-surface interface giving rise to an apparent fluid slip (or reduced wall shear stress than would otherwise be expected). The slip-length is defined as the ratio of slip-velocity to shear rate at the wall, or a virtual distance into the wall at which the liquid velocity vanishes to zero when linearly extrapolated as shown schematically in Figure 1B.[1] The reduction of superhydrophobicity during the rheological testing, through degradation of surface roughness, and/or loss of the trapped air layer, is detected as a decrease in the measured slip-length in real-time.

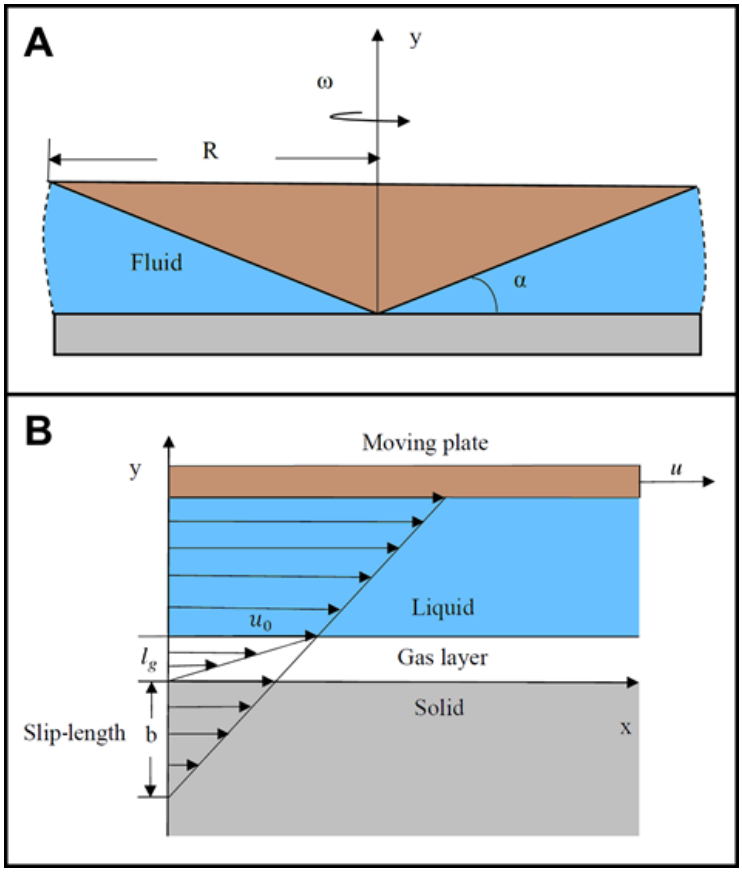

Figure 1. Schematic diagrams of slip-length measurement. (**A**) An illustration of the cone-and-plate rheometer system, where **ω** is the angular velocity, **R** is the radius of the cone-and-plate, and **α** is the angle of the cone. (**B**) A slip-length concept illustration, where $\boldsymbol{u}/\boldsymbol{u_0}$ are the velocities of the cone/liquid, $\boldsymbol{l_g}$ is the thickness of the gas layer, **b** is the slip-length, and **x** is the planar axis of the solid surface. Additionally, **y** is the central rotational axis for both parts.

This study utilises two types of prototypical superhydrophobic materials surfaces to demonstrate this rheological testing method; (i) systematically engineered polytetrafluoroethylene (PTFE), and (ii) nanoparticulate surface coatings - both providing different degradation behaviours.[3,37,38] The testing method is shown to provide quantifiable measurement of superhydrophobic robustness, and longevity. Indicating the real-world persistence of these materials via dynamic testing conditions. Wider implementation of this class of analysis would allow for the universal comparison of materials, accelerating the design of more robust superhydrophobic surfaces, able to function reliably in real-world conditions.

2. Experimental Set-up

2.1 Manufacture of superhydrophobic xPTFE surface

Superhydrophobicity is created *via* a combination of micro/nano-scale surface structures and a low surface free energy material, PTFE.[37,38] In this work, a simple and inexpensive method to create superhydrophobicity on a PTFE surface is utilized. This method is based on the transference of structures from very fine stainless-steel meshes onto the PTFE sheets. PTFE was chosen due to its low surface free energies, low coefficient of friction, and flexibility.[39] Microscale diameter stainless-steel meshes were used to emboss the PTFE sheets (Full details provided in Supplementary Information).

2.2 Manufacture of superhydrophobic TiO_2 Surface

The TiO_2 coatings were fabricated using a two-step process; (i) hydrophobic adhesive, followed by (ii) surface roughening using hydrophobic titanium dioxide nanoparticles. Both steps were carried out using spray coating to ensure conformal surface coverage (Full details provided in Supplementary Information).

2.3 Slip-length measurements

Previous studies on similar superhydrophobic surfaces suggest the potential slip-length for both types of surfaces should be around 10-100 microns (i.e. on the order of the "large" scale surface structure).[37,38] For such small lengths, a rheometer is a good choice for slip-length measurement due to its high accuracy and well-controlled viscometric flow field. The rheometer used here is a torque controlled, compressed air bearing system and measures the angular velocity (at fixed torque) to determine the fluid viscosity. In this work, the slip-lengths were measured by an Anton Paar MCR 302 rheometer with a cone-and-plate measuring system (with a cone angle of 1° and radius of 3 cm, unless otherwise stated). The rheometer has a measurable torque range from 1 to 200 nN·m with a resolution of 0.1 nN·m.

In a cone-and-plate set up when both surfaces exhibit "no-slip" boundaries, the shear rate is constant, resulting in a viscometeric Couette flow which is simple and can be calculated analytically neglecting any inertial or edge effects. The torque in this case is then:

$$T = \frac{2}{3}\pi\mu\frac{\omega}{\tan\alpha}R^3 \quad [1]$$

Where T is the torque acting on the cone-and-plate, μ is the viscosity of the fluid, ω is the angular velocity, α is the angle of the cone and R is the radius of the cone-and-plate.[40] If the lower no-slip plate is replaced by a superhydrophobic surface with a slip-length of b, the torque with slip T_s is:[41]

$$T_s = \frac{2}{3}\pi\mu\frac{\omega}{\tan\alpha}R^3\cdot\left[\begin{array}{l}1-\frac{3}{2}\cdot\frac{b}{\tan\alpha\cdot R}+3\left(\frac{b}{\tan\alpha\cdot R}\right)^2 \\ -3\left(\frac{b}{\tan\alpha\cdot R}\right)^3\times\ln\left(1+\frac{\tan\alpha\cdot R}{b}\right)\end{array}\right] \quad [2]$$

Setting:

$$s = \frac{b}{\tan\alpha\cdot R} \quad [3]$$

The "drag reduction" can then be defined as:

$$Dr = \frac{T_0 - T_s}{T_0} = \frac{3}{2}\cdot s - 3s^2 + 3s^3\cdot\ln\left(1+\frac{1}{s}\right) = \frac{\mu_{ba} - \mu_{ap}}{\mu_{ba}} \quad [4]$$

Where μ_{ap} is the apparent viscosity measured on the superhydrophobic surfaces, and μ_{ba} is the known (baseline) viscosity of the fluid. Hence the slip-length can be determined from the apparent viscosity measured on the superhydrophobic surfaces. It is worth noting that for the slip-length measurements the shear rate range was chosen to be lower than 500 1/s to avoid any inertial effects and an acrylic ring was used to trim the free surface to minimize surface tension effects. The instrument was operated using automatic shear rate adjusting time, whereby the shear rate constant until the measuring point is generated. The maximum adjusting time was five seconds.

2.4 Shear stress creep experiments

A range of working fluids was selected to cover as wide a shear stress range as possible. For stresses in the range 0.06 Pa to ~2.2 Pa, the working fluid selected was water, for a range of intermediate stresses ~2-18 Pa, a 12% PEG solution (~7 mPa.s) was utilised and, for the TiO_2 surfaces a highly viscous 47% PEG solution (~285 mPa.s) was used to extend the range still further. Each shear stress was applied for 90 s then the slip-lengths were measured. For a single experiment this included 15 steps, therefore a total time of 22.5 mins was expected for each test. As it is well known that the slip-length is a function of viscosity,[42] a correction was used

in order to determine the "viscosity corrected slip-length (Slip-length*) *via* normalisation of the measured slip-length by the slip-length of water. In this manner, the effects of different fluid viscosities could be approximately accounted for and good agreement was observed for this normalised slip-length at identical shear stresses for different fluids.

2.5 Time endurance experiments

The time endurance of the superhydrophobic surfaces were tested by applying a constant fluid shear stress for extended periods of time. The experiments used a smaller (α = 2°, R = 1 cm) cone geometry, ensuring numerous tests could be performed for a given surface dimension (typically 10 cm x 10 cm for each surface). The superhydrophobicity over time was examined by intermittently measuring the static WCA, and the slip-length. Any resulting damage to the surface structures was observed using scanning electron microscopy (SEM) imaging. The critical shear stresses of the xPTFE surfaces (~1 Pa) was used for the starting point for time endurance tests, exposing the samples for 8 hours using; 1 Pa, 5 Pa, and 10 Pa of fluid shear stress. For the TiO_2 surfaces, higher stresses were required to cause surface damage.

2.6 Materials Characterisation Techniques

SEM imaging was performed using a field emission microscope (JEOL, JSM-7001F) using an acceleration voltage of 5 kV. The samples were coated (sputtered) with a fine layer (~ 5 nm) of chromium to prevent sample charging. WCA measurements were performed using a Kruss (DSA100E) Drop Shape Analyser. Water droplet volumes were maintained at 3 μL, the WCA values were observed directly, and repeated six times for each material. Water bouncing experiments were carried out using 8 μL water droplets released from a 20 mm height, and imaged using a Sony RX10 III camera with images captured at 1000 frames per second.[43]

3. Results and Discussion

3.1 Materials

The two materials utilised in this study (xPTFE, and TiO_2 coatings) were manufactured using hot-embossing and spray-coating techniques respectively. The wetting properties of each material were fully characterised (Table 1), in addition SEM imaging was used to assess "virgin"

morphology. The micro-roughness of the xPTFE surfaces provided a surface with WCA of 145°, with a WCA hysteresis of 16°. The superhydrophobic TiO_2 coatings provided WCA of 165°, with a WCA hysteresis of 6°. Water bouncing experiments were used to access dynamic surface wetting; the lower water repellence of the xPTFE provided on average a single bounce, whereas the TiO_2 coatings demonstrated an average of 12 bounces. These results confirm the exceptional superhydrophobicity of the TiO_2 coatings, but also suggest the xPTFE material has superhydrophobic character, even though the static WCAs are below 150°.[43,44]

Table 1. Properties summary of the hydrophobic surfaces.

	xPTFE surface	**TiO_2 surface**
Static WCA	145°±5°	165°±5°
Advancing WCA	152°±3°	168°±2°
Receding WCA	135°±3°	162°±3°
WCA Hysteresis	16°	6°
Features Size	30±3 μm	25±5 nm (*minimum*)
Slip-length	27±3 μm	55±3 μm

Both materials have a similar surface chemistry (fluoroalkyl; xPTFE – PTFE, and TiO_2 – fluoroalkylsilane), and so the differences in wetting behaviour stem mostly from the surface roughnesses. Both materials have a dual-scale surface roughness, with xPTFE consisting of micro-pillars topped with microfibers (Figure 2B), and the TiO_2 surfaces consisting of micro agglomerations of nanoparticles (Figure 2D) – the latter providing extremely high surface roughness.

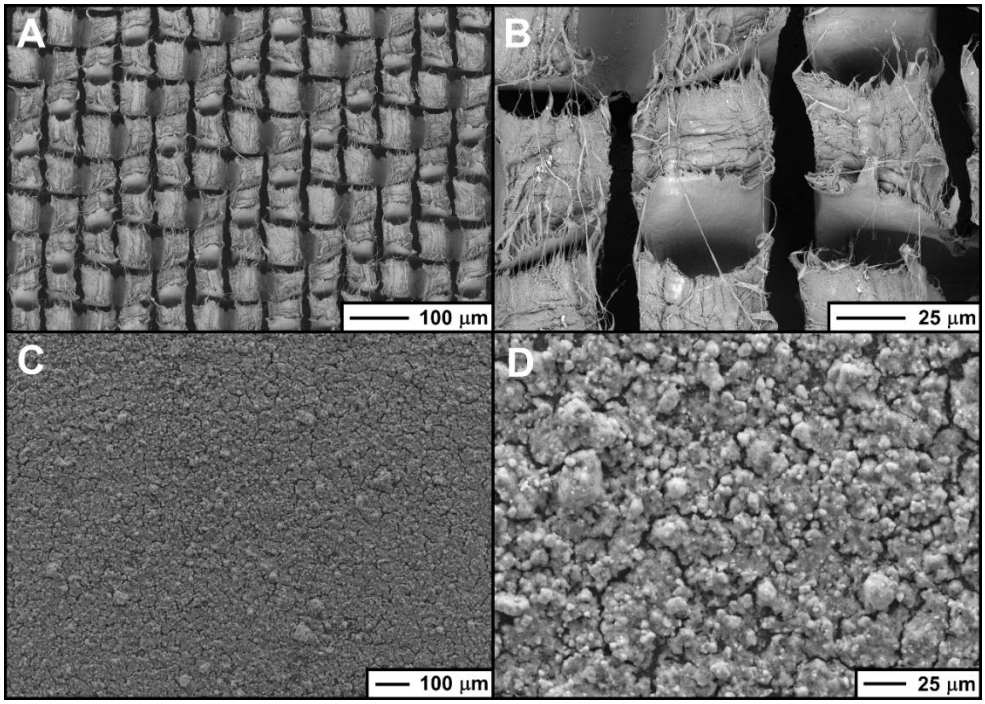

Figure 2. SEM images of xPTFE (**A/B**), and TiO_2 surfaces (**C/D**). Scale bars are shown.

3.2 Slip Length Characterisation

The superhydrophobicity of each material is further quantified using its slip-length as shown in Figure 3, which is a measure of the reduction in apparent viscosity of a measured liquid, brought about by superhydrophobic drag reduction (i.e. an apparent slip layer next to the surface, Figure 1B). Using water, for both xPTFE and TiO_2 surfaces, the apparent viscosity is reduced significantly below the value measured from the baseline test (which itself is in excellent agreement with the textbook value).[40] The xPTFE surfaces showed a drag reduction of around 7.0%, which is equivalent to a slip-length of 27 μm. The TiO_2 surfaces provide a drag reduction of 13.3%, which indicates a slip-length of 55 μm. These measurements stem from the disparity in the surface hydrophobicity (such as WCA, or number of droplet bounces), and feature size of each material. The use of slip-length to characterise superhydrophobicity allows for testing of a larger surface region, relative to static WCA, or droplet bounces. It is also a direct measure of the surface's drag reduction capability, which is not consider in static measurements. This results in higher reproducibility, and a lower uncertainty in the measurement.

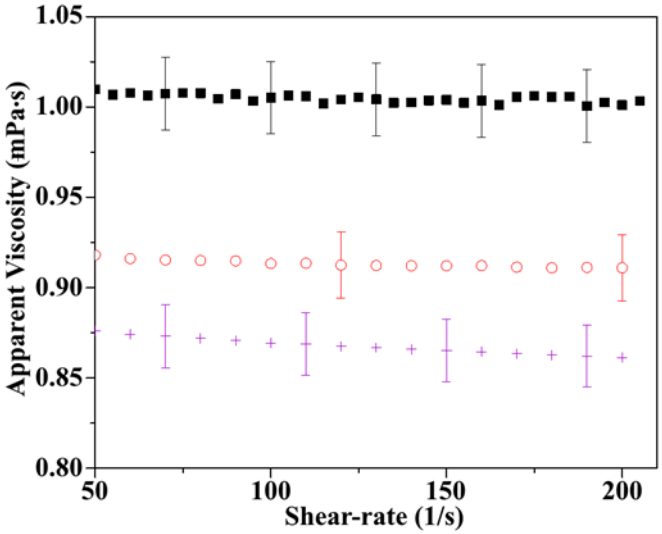

Figure 3. Slip-length measurement for superhydrophobic surfaces (■ water baseline using polished stainless steel surface, b = 0 μm, ○ xPTFE surface, b = 27 μm, and + TiO_2 surface, b = 55 μm). The error bars represent the variation of repeats.

3.3 Shear-stress creep experiments

The shear stress test is a controlled quantitative measure of surface wear *via* fluid shear, providing repeatable analysis through the testing of a relatively large surface area. The use of fluids also provides a more representative understanding of 'in-use' wear (e.g. drag-reducing surfaces), relative to arbitrary physical abrasion (e.g. scratch / adhesive tape testing).

The combination of using different fluids with different shear viscosities, and varying the shear rate, meant that a wide range of fluid shear stress (0.1 Pa to 1000 Pa) could be applied to the superhydrophobic surfaces. Three working fluids are used in the experiments for different range of shear stress including distilled water, and two polyethylene glycol (PEG) solutions with different concentrations (12% and 47%, w/w). The PEG polymer used has a molecular weight of 8000 Da (PEG8000), and essentially is a viscous Newtonian solution (Dontula et al. (1998)). The shear viscosities of these two fluids are 7.1 mPa·s and 285 mPa·s at 20°C for the 12% and 47% concentrations respectively. As is well known, the slip-length increases with the fluid viscosity and is assumed to be independent of the shear rate (confirmed in Figure 3).[42,45] Figure 4 (inset) shows how viscosity increases the slip-length for the two surfaces studied here. In order to make fair comparisons across different fluids we therefore plot the equivalent water "slip-length*" (i.e. the slip-lengths were divided by 1.48 (for xPTFE surfaces)/1.6 (for TiO_2 surfaces) and 2.36 for 12% PEG8000 and 47% PEG 8000 respectively).

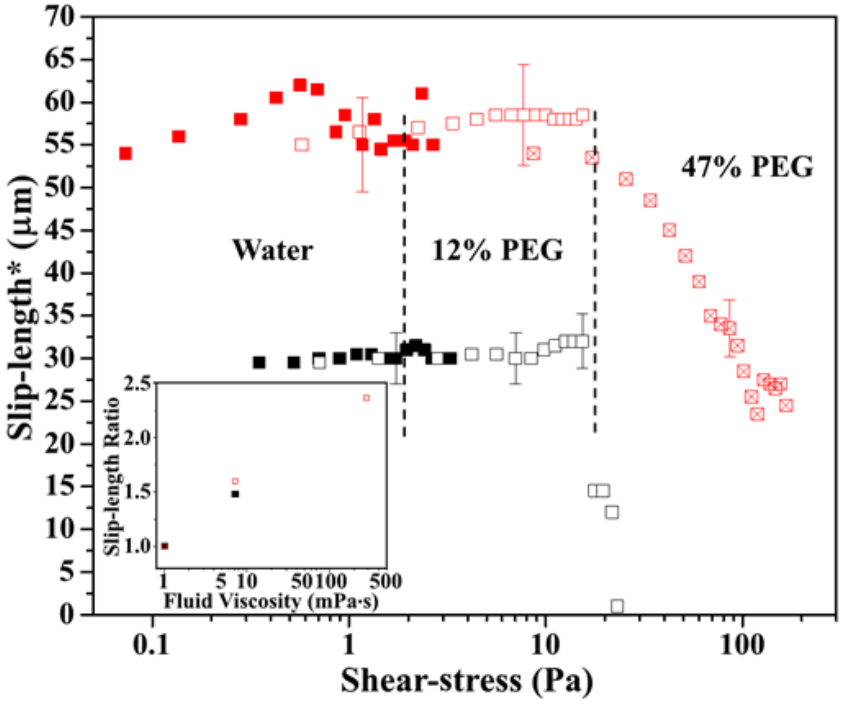

Figure 4. Shear-stress experiments for (black) xPTFE surfaces and (red) TiO_2 surface using water (■), 12% PEG8000 (□) and 47% PEG 8000 (☒) solutions in a cone-and-plate geometry (α = 1°, R = 3cm). The error bars represent the variation of repeats. The inset figure shows the variation of the ratio of actual slip-length divided by the slip-length of water against fluid viscosity.

Figure 4 shows the shear stress creep results of both surfaces. For the xPTFE surface the fluid shear stress was extended to 17.8 Pa using 12% PEG8000 (0.6 Pa ~ 17.8 Pa) due to its higher resilience and no slip-length loss was observed during these water tests. The xPTFE shows a partial loss of the superhydrophobicity occurred when the fluid shear stress was around 15 Pa, and a complete loss of superhydrophobicity when this approached 25 Pa. The slip-length of xPTFE surfaces can be partially recovered to 15 ~ 20 μm after cleaning using water and allowing to dry naturally. This recovery is due to the mechanism of superhydrophobicity loss – for the xPTFE the main cause is the removal of trapped air at the interface. The air layer is reintroduced when the material is washed and dried, with the incomplete recovery of slip-length, a result of partial surface damage.

The resilience testing of the more superhydrophobic TiO_2 surfaces required extension of the fluid shear stress to significantly higher values (0.1 Pa ~ 200 Pa). A higher concentration of PEG fluid (47% PEG) was required to achieve this greater stress. The results of these shear stress step tests for TiO_2 surfaces are shown in Figure 4. The resilience of the TiO_2 against the low-medium shear stress wear is observed to be much better than the xPTFE surfaces. Its

superhydrophobicity decreases only when the fluid shear stress is over 20 Pa. Hence, the critical shear stress to cause a partial loss of superhydrophobicity was identified as ~25 Pa for the TiO_2 surface.

It should be noted that even when fluid shear stress was increased to around 200 Pa, the TiO_2 surfaces were able to maintain a slip-length of around 15 μm. Suggesting that even at these elevated stresses the superhydrophobic character was not completely lost, through only partial surface structure damage, or only partial removal of trapped air. This resilience stems from the structure of the TiO_2 coating, as it consists of agglomerations of nanoparticles (smallest diameter ~25 nm) combined with adhesives and hydrophobic binders, the varied size of the particle groups results in a more complicated surface structure (shown in Figure 2). This result indicates that particular regions of the nanoparticle coating exhibit higher resilience.

3.4 Time endurance experiments

The critical shear stress provides an insight into the material's maximal stress resilience. In order to gain a comprehensive understanding of 'in-use' resilience, time endurance was also tested. This was carried out by applying a constant fluid shear stress for extended periods of time. The superhydrophobicity was examined by measuring the static WCA and the slip-length. Any damage to the surface structures was observed using SEM imaging. The surfaces were exposed to a series of fluid shear stresses (1, 10 Pa for both surfaces, and 100 Pa for TiO_2) for 8 hours, as this probes the full range of resilience probed by the critical shear stress experiments (Figure 5).

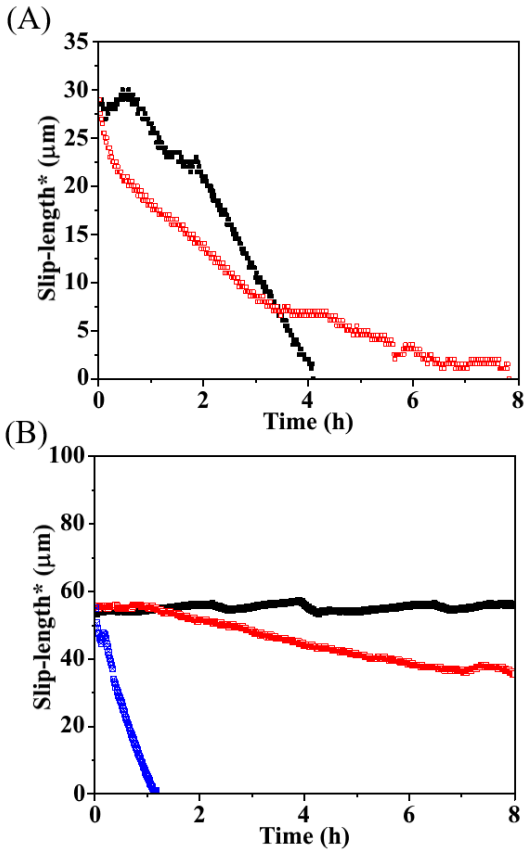

Figure 5. Representative time endurance data for (a) xPTFE surfaces under 1Pa (■) and 10Pa (□) for 8 hours, using water and 12% PEG8000 solution in a cone-and-plate geometry (α = 2°, R = 1cm). (b) TiO_2 surfaces under 1Pa (■), 10Pa (□) and 100Pa (⊠) for 8 hours, using water, 12% PEG8000 and 47% PEG8000 solutions *via* a cone-and-plate geometry (α = 2°, R = 1cm).

xPTFE. The xPTFE surfaces (Figure 5A) showed moderate resilience to a 1 Pa fluid shear stress. Where the surfaces maintained its superhydrophobicity in the first hour, then its slip-length decreased rapidly and disappeared within 4 hours. The static WCA were measured as 145°±5° for fresh surfaces, which decreased to 130°±10° after the wear. The static WCA varied greatly at different positions on the surface, indicating that the loss of superhydrophobicity is spatially non-uniform and that, some part of the surface was still superhydrophobic. The changes of the surface structures, observed via SEM after 8 hours of 1 Pa fluid shear stress, are shown in Figure 6 [A(i) / B(i)]. The changes to the surface structure of the xPTFE surfaces are seen as the removal of the "hair-like" structures after the wearing process, in addition to abrasion to the top of each protrusion causing wear and smoothing. The relative ratios of the protrusion tops increased from 54% to 66% upon testing. These changes indicate a permanent loss of superhydrophobicity.

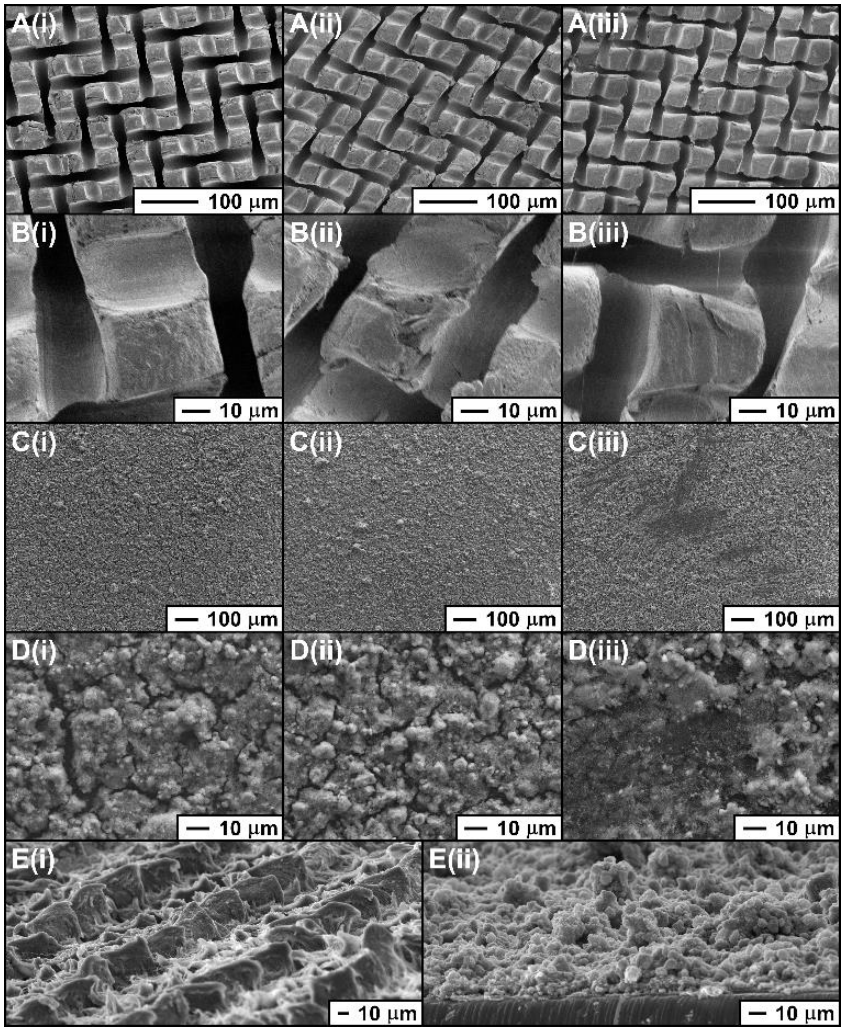

Figure 6. SEM images of (A/B) xPTFE and (C/D) TiO_2 surface after various shear stresses; (i) 1 Pa, (ii) 5 Pa (xPTFE), 10 Pa (TiO_2), and (iii) 10 Pa (xPTFE), 100 Pa (TiO_2), for 8 hours. Static WCA for each material (after 8 hours of testing) follow - xPTFE; (1 Pa) 130°, (10 Pa) 122°, and TiO_2; (1 Pa) 162°, (10 Pa) 157°, (100 Pa) *highly varied* ~91-157°. (E) Side-on SEM of (i) xPTFE, and (ii) TiO_2 surfaces. Scale bars are shown in each image.

Exposing the xPTFE surfaces to a higher 10 Pa fluid shear stresses resulted in a similar amount of visible damage, shown by an increase in the open area ratio from 54% to 66% after 8 hours. The static WCAs were measured as 122°±22° after this testing, which is lower than that observed for a 1 Pa shear stress (WCA of 130°). To more clearly quantify the loss of superhydrophobicity, the slip-length loss per unit time verses fluid shear stress was calculated, as shown in Figure 7. Four repeat measurements were conducted for each stress and surface combination. Generally, this quantity was shown to increase as the fluid shear stress was also increased.

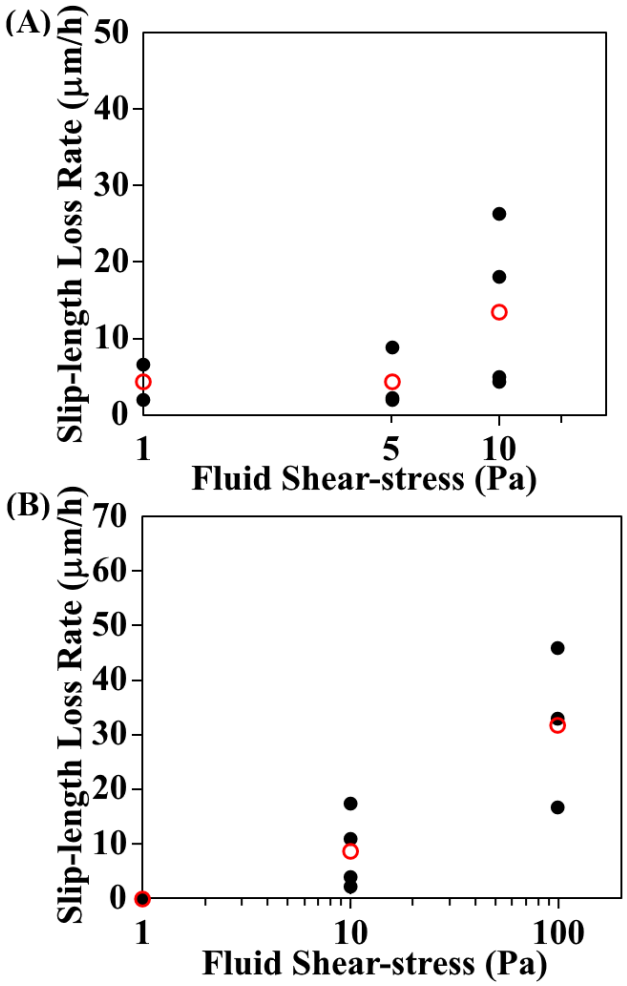

Figure 7. Slip-length loss rate vs fluid shear stress of (**A**) xPTFE surface and (**B**) TiO_2 surface, (•) data for single experiment, (○) average values.

Further SEM characterisation of the xPTFE surfaces exposed to different fluid shear stresses showed similar wear behaviour, but to differing degrees (Figure 6, with the most abraded cases shown in A/B(iii)). The edges and the top of the posts were polished, in addition to a complete removal of the pillar microfibers, and sandpaper scratches applied during the manufacture process.

The slip-length loss rate presented a large variation for each fluid shear stress (Figure 7). The wear of 1 Pa shear stress resulted in a loss of slip-length ranging from 1 to 6 μm/h and the average value is around 3 μm/h which indicates that the surface could lose all of its superhydrophobicity within about 10 hours. When the shear stress increased to 5 Pa, the average and the maximum value of the slip-length loss rate reached 6 μm/h and 9 μm/h respectively. The time endurance of its superhydrophobicity decreases to between 3 to 5 hours

under this condition. For the 10 Pa fluid shear stress, the average and the maximum value of the slip-length loss rate increased to 14 μm/h and 27 μm/h respectively, the superhydrophobicity of the xPTFE surfaces at this stress can be maintained for 1 to 2 hours.

TiO_2. TiO_2 surfaces showed a higher resilience than the xPTFE surface, and required higher fluid shear stress for the time endurance study. Utilising distilled water, 12% PEG and 47% PEG fluids to create 1 Pa, 10 Pa and 100 Pa fluid shear stresses in this test respectively (Figure 5). From the results, the slip-length of the TiO_2 surfaces essentially kept the same during the application of a 1 Pa fluid shear stress wear. This is reflected in the examination of the SEM image (Figure 6), which shows no observable difference relative to the fresh surfaces (Figure 2). While the static WCAs were measured as 162°±3° on the surfaces after the testing, compared to 165° on the fresh surfaces.

When the fluid shear stress increased to 10 Pa, the slip-length started to decrease linearly with time after 1 hour of stress. After 8 hours, the slip-length was measured as around 40 μm. The static WCAs were 157°±3°, and no significant variations in wetting across different positions on the surface were observed. SEM images (Figure 6) showed no major difference, relative to the fresh surface. After 8 hours of a 10 Pa fluid shear stress, the TiO_2 surface had only partly lost its superhydrophobicity (Figure 5), and the remaining structures were still uniform.

When the fluid shear stress increased to 100 Pa, the slip-length decreased rapidly and vanished in about 1 hour. After testing, the static WCAs were extremely varied (~91°-157°), which indicated that some parts of the surface had entirely lost superhydrophobicity, and the surface was no longer uniform. The change to the surfaces were obvious after the experiments, a few "large" scratches on the surface were observed even by the naked-eye. From the SEM images at different magnifications, as shown in Figure 6, the widths of these obvious scratches can be measured as hundreds of microns. The TiO_2 coating was totally abraded at these positions on the surface resulting in a considerable damage to the surface structure. The images with higher magnification at these locations showed the micro/nano scale structures were smoothed and damaged, and the remaining roughness of the surface was no longer providing superhydrophobicity.

The slip-length loss per unit time on TiO_2 surfaces (Figure 7) showed no loss of the slip-length observed during the 1 Pa fluid shear stress wear, but it increased with the higher fluid shear stress. When the shear stress increased to 10 Pa, the average and the maximum value of the

slip-length loss rate reached 9 μm/h and 17 μm/h respectively. These surfaces showed a better resilience than the xPTFE surfaces in the same condition. For the 100 Pa fluid shear stress, the average and the maximum value of the slip-length loss rate increased to 32 μm/h and 46 μm/h respectively, their superhydrophobicity could only remain for 1 to 2 hours.

Comparing the two materials, the xPTFE shows a lower resilience to the type of shear stress applied in this study. This is demonstrated by looking at the slip-length for both materials when a 10 Pa shear stress is applied. The xPTFE slip-length falls rapidly over a few hours, but the superhydrophobic TiO_2 surface is only partially reduced when the same stress is applied (Figure 5) – in addition to showing no appreciable signs of surface damage. The TiO_2 surfaces maintains a non-zero slip-length for over one hour even when a fluid shear stress of 100 Pa is applied.

The difference in slip-length behaviour is a direct measure of the material's superhydrophobicity, and potential as a 'drag reduction' surface. A consequence of the surface roughness, surface chemistry, and presence/stability of trapped air at the water-surface interface. The micro-roughness of the PTFE, provides an overall lower hydrophobicity (demonstrated by lower static WCAs, and number of water bounces supported), but also allows for easier removal of the trapped air. This is shown by the partial regain of WCA in the xPTFE samples after shear stress testing, in addition to the limited damage (partial feature smoothing) of the micro-pillars using a 10 Pa shear stress. The micro/nano-roughness of the TiO_2 surfaces is more resilient by design, whereby the air is trapped within the material's nano-porosity – hence harder to remove.[46] Visible damage to the surface is only seen when a high shear stress is applied (100 Pa).

Additional experiments were carried out using PTFE to explore the mechanism of air loss. This included materials with; (i) larger pillars, and a low proportion of trapped air, and (ii) smaller pillars, with a higher proportion of trapped air (30040, and 50025 xPTFE respectively – Supplementary Information Figure S1). In both examples, the materials performed poorly in shear stress creep experiments, when compared to the xPTFE described throughout this manuscript (Supplementary Figure S2). Both demonstrating a zero slip-length below a 2 Pa shear stress, compared to ~15 Pa demonstrated in the original material. However, all three PTFE materials performed comparably in 1 Pa shear stress time endurance (Supplementary Figure S3). Therefore, the slip-length testing reveals that the morphology of the xPTFE materials (square pillars fabricated from hydrophobic material), provides a similar resilience

to low intensity perturbation – with a steady loss of trapped air from the interface. Additionally, when higher shear stresses are applied in the creep experiments, a maximum tolerance level can be observed – where the immediate removal of trapped air occurs, and the slip-length falls to zero. Both additional samples show total air removal at lower shear stresses for differing reasons. The 30040 xPTFE, provides a lower proportion of trapped air, but also a higher proportion of flat areas (pillar tops) – this results in more Wenzel-type wetting mechanism.[18] This allows for more rapid ingress of wetting when higher shear stresses are applied. The 50025 xPTFE, provides a higher proportion of trapped air which is more easily accessible, and can be easily removed under shear stress testing. Testing of these morphologies, demonstrates that additional understanding can be gained from slip-length testing – and its relevance to evaluating hydrophobic material resilience.

Conclusions

The investigation of surface resilience using slip-length measurement provides comprehensive characterisation of the superhydrophobic nature of a material. Building upon the information gathered using conventional static WCA, WCA hysteresis, and even water bouncing experiments. The reported technique allows for a more conclusive superhydrophobic characterisation, relative to WCA – which have been shown to be highly dependent on the method of characterisation.[12] Slip-length resilience delivers analysis that could provide straightforward comparison across the spectrum of superhydrophobic materials generated. Not solely evaluating baseline superhydrophobicity, and drag reduction potential (through slip-length analysis), but the potential for its real-world application (through slip-length resilience).

Conflicts of interest

There are no conflicts to declare.

Acknowledgements

RJP would like to thank the Engineering and Physical Sciences Research Council (EPSRC) for the award of a Fellowship under grant EP/M025187/1. CRC would like to acknowledge the Royal Society ‘Research Grant’ Scheme for funding.

Notes and references

1. C. Lee, C.-H. Choi and C.-J. Kim, *Exp. Fluids*, 2016, **57**, 176.
2. E. Huovinen, L. Takkunen, T. Korpela, M. Suvanto, T. T. Pakkanen and T. A. Pakkanen, *Langmuir*, 2014, **30**, 1435–1443.
3. Y. Lu, S. Sathasivam, J. Song, C. R. Crick, C. J. Carmalt and I. P. Parkin, *Science*, 2015, **347**, 1132–1135.
4. G. D. Bixler, A. Theiss, B. Bhushan and S. C. Lee, *J. Colloid Interface Sci.*, 2014, **419**, 114–133.
5. C. R. Crick, S. Ismail, J. Pratten and I. P. Parkin, *Thin Solid Films*, 2011, **519**, 3722–3727.
6. E. Ozkan, C. R. Crick, A. Taylor, E. Allan and I. P. Parkin, *Chem. Sci.*, 2016, **7**, 5126–5131.
7. C. R. Crick, J. A. Gibbins and I. P. Parkin, *J. Mater. Chem. A*, 2013, **1**, 5943–5948.
8. W. Zhou, G. Li, L. Wang, Z. Chen and Y. Lin, *Appl. Surf. Sci.*, 2017, **413**, 140–148.
9. N. Wang, D. Xiong, Y. Deng, Y. Shi and K. Wang, *ACS Appl. Mater. Interfaces*, 2015, **7**, 6260–6272.
10. L. Ionov and A. Synytska, *Phys. Chem. Chem. Phys.*, 2012, **14**, 10497–10502.
11. X. Tian, T. Verho and R. H. A. Ras, *Science*, 2016, **352**, 142–143.
12. C. R. Crick and I. P. Parkin, *Chem. – Eur. J.*, 2010, **16**, 3568–3588.
13. B. Su, Y. Tian and L. Jiang, *J. Am. Chem. Soc.*, 2016, **138**, 1727–1748.
14. D. Zhi, Y. Lu, S. Sathasivam, I. P. Parkin and X. Zhang, *J. Mater. Chem.* A, 2017, **5**, 10622-10631.
15. P. Wang, D. Zhang, S. Sun, T. Li and Y. Sun, *ACS Appl. Mater. Interfaces*, 2017, **9**, 972-982.
16. X. Tian, S. Shaw, K. R. Lind and L. Cademartiri, *Adv. Mater.*, 2016, **28**, 3677-3682.
17. F. Schellenberger, N. Encinas, D. Vollmer and H.-J. Butt, *Phys. Rev. Lett.*, 2016, **116**, 96101.
18. R. N. Wenzel, *Ind. Eng. Chem.*, 1936, **28**, 988–994.
19. A. B. D. Cassie and S. Baxter, *Trans. Faraday Soc.*, 1944, **40**, 546–551.
20. D. Quéré and M. Reyssat, *Philos. Trans. R. Soc. Lond. Math. Phys. Eng. Sci.*, 2008, **366**, 1539–1556.

21. N. J. Shirtcliffe, G. McHale, S. Atherton and M. I. Newton, *Adv. Colloid Interface Sci.*, 2010, **161**, 124–138.
22. L. Boinovich, A. M. Emelyanenko and A. S. Pashinin, *ACS Appl. Mater. Interfaces*, 2010, **2**, 1754–1758.
23. S. A. Mahadik, P. D. Fernando, N. D. Hegade, P. B. Wagh and S. C. Gupta, *J. Colloid Interface Sci.*, 2013, **405**, 262–268.
24. D. Quéré, *Annu. Rev. Mater. Res.*, 2008, **38**, 71–99.
25. T. Verho, C. Bower, P. Andrew, S. Franssila, O. Ikkala and R. H. A. Ras, *Adv. Mater.*, 2011, **23**, 673–678.
26. A. Milionis, E. Loth and I. S. Bayer, *Adv. Colloid Interface Sci.*, 2016, **229**, 57–79.
27. X. Deng, L. Mammen, H.-J. Butt and D. Vollmer, *Science*, 2012, **335**, 67–70.
28. H. Wang, Y. Xue, J. Ding, L. Feng, X. Wang and T. Lin, *Angew. Chem. Int. Ed.*, 2011, **50**, 11433–11436.
29. L. Wu, J. Zhang, B. Li, L. Fan, L. Li and A. Wang, *J. Colloid Interface Sci.*, 2014, **432**, 31–42.
30. J. Groten and J. Rühe, *Langmuir*, 2013, **29**, 3765–3772.
31. H. Wang, H. Zhou, A. Gestos, J. Fang and T. Lin, *ACS Appl. Mater. Interfaces*, 2013, **5**, 10221–10226.
32. R. Hensel, A. Finn, R. Helbig, H.-G. Braun, C. Neinhuis, W.-J. Fischer and C. Werner, *Adv. Mater.*, 2014, **26**, 2029–2033.
33. Y. Zhang, D. Ge and S. Yang, *J. Colloid Interface Sci.*, 2014, **423**, 101–107.
34. A. Davis, Y. H. Yeong, A. Steele, E. Loth and I. S. Bayer, *RSC Adv.*, 2014, **4**, 47222–47226.
35. A. Davis, Y. H. Yeong, A. Steele, E. Loth and I. S. Bayer, *AIChE J.*, 2014, **60**, 3025–3032.
36. Z. Lu, P. Wang and D. Zhang, *Corros. Sci.*, 2015, **91**, 287–296.
37. H. Xu, A. Clarke, J. P. Rothstein and R. J. Poole, *Appl. Phys. Lett.*, 2016, **108**, 241602.
38. H. Xu, A. Clarke, J. P. Rothstein and R. J. Poole, *J. Colloid Interface Sci.*, 2018, **513**, 53–61.
39. E. L. Decker and S. Garoff, *Langmuir*, 1997, **13**, 6321–6332.
40. H. A. Barnes, J. F. Hutton and K. Walters, Eds., in *An Introduction to Rheology*, Elsevier, 1989, vol. 3.
41. A. Lee, C.-H. Choi and C.-J. 'CJ' Kim, *Phys. Rev. Lett.*, 2008, **101**, 64501.

42. S. Srinivasan, W. Choi, K.-C. Park, S. S. Chhatre, R. E. Cohen and G. H. McKinley, *Soft Matter*, 2013, **9**, 5691–5702.
43. C. R. Crick and I. P. Parkin, *Chem. Commun.*, 2011, **47**, 12059–12061.
44. C. R. Crick and I. P. Parkin, *J. Mater. Chem. A*, 2013, **1**, 799–804.
45. C.-H. Choi and C.-J. Kim, *Phys. Rev. Lett.*, 2006, **96**, 66001.
46. M. J. Mayser and W. Barthlott, *Integr. Comp. Biol.*, 2014, **54**, 1001–1007.